JOURNAL OF GEOPHYSICAL RESEARCH, VOL. 96, NO. C2, PAGES 2661–2673, FEBRUARY 15, 1991

An Investigation of Short-Range Climate Predictability in the Tropical Pacific

MOJIB LATIF AND MORITZ FLÜGEL

Max-Planck-Institut für Meteorologie, Hamburg, Federal Republic of Germany

The predictability of the El Niño/Southern Oscillation (ENSO) phenomenon was investigated by analyzing observed sea levels, surface stresses, and subsurface temperatures simulated with an oceanic general circulation model forced by observed winds. In addition, a large ensemble of prediction experiments has been conducted with a simplified coupled ocean-atmosphere model consisting of an oceanic general circulation model coupled to a simple atmospheric feedback model. Our analysis supports the hypothesis that the ENSO-related interannual variability in the tropical Pacific can be understood as a cycle within the coupled ocean-atmosphere system which is inherently predictable. This cycle consists of an accumulation of warm water in the western Pacific during the cold phases of ENSO and a loss of this heat during its warm phases. The results of the prediction experiments with our simplified coupled ocean-atmosphere model indicate that the phase of tropical Pacific sea surface temperatures is predictable two to three seasons in advance with our simplified coupled system, whose dynamics is governed by the ocean. We found a strong dependence of the skills on season, with spring SSTs being least predictable.

1. INTRODUCTION

Interannual variability in the tropical Pacific is dominated by the El Niño/Southern Oscillation (ENSO) phenomenon [e.g., *Wyrtki*, 1975; *Cane*, 1986], which arises from a slowly evolving instability of the coupled ocean-atmosphere system. In mid-latitudes, instabilities of either the atmospheric or oceanic circulation generally limit the predictability of the climate system. In the tropics, however, the instability of the coupled ocean-atmosphere system plays an important role in determining the quasi-periodic nature of the low-frequency variability, which provides a basis for long-range predictability in this region.

Although the ENSO mechanism is not yet fully understood, there is growing evidence from observation and modeling studies that ENSO is associated with slow variations in the equatorial heat content as described by *Wyrtki* [1985]. He hypothesized that prior to warm events a slow buildup of warm water takes place in the western equatorial Pacific up to a certain point, when the warm water pool becomes unstable. This water is then released toward higher latitudes during the El Niño event. The period between El Niños is related to the time which is required to refill the equatorial heat reservoir. *Zebiak and Cane* [1987] attribute the interannual variability simulated with their coupled ocean-atmosphere model to essentially the same mechanism. *Battisti* [1988] primarily attributes the interannual variability simulated in the same coupled model to ocean wave dynamics known as the "delayed action oscillator" [*Schopf and Suarez*, 1988], according to which the reversal between El Niño (warm) and La Niña (cold) conditions is caused by the propagation of internal equatorial Rossby waves and their reflection at meridional boundaries. The importance of off-equatorial Rossby waves within this concept is described by *Graham and White* [1988], who investigated observational and model data. Their findings are consistent with an earlier model study of *McCreary* [1983]. Common to all of these studies is the description of ENSO as a cycle within the tropical Pacific, which implies its "a priori" predictability.

Further evidence for the predictability of ENSO comes from several uncoupled model simulations. It is well known that changes in certain oceanic key variables of ENSO, such as sea level or sea surface temperature (SST), are primarily caused by changes in the ocean dynamics forced by changes in the surface wind field, rather than by changes in the surface heat flux [e.g., *Bjerknes*, 1969; *Wyrtki*, 1975]. It could be shown that the observed low-frequency changes in sea level can already be simulated realistically with relatively simple ocean models using observed wind stresses [*Busalacchi and O'Brien*, 1981; *Busalacchi et al.*, 1983] and that these changes are consistent with the propagation of baroclinic equatorial waves. In more recent studies, general circulation models of the ocean (OGCMs) have been used in the hindcast mode, prescribing observed wind stress distributions [e.g., *Philander and Seigel*, 1985; *Latif*, 1987; *Seager*, 1989] and have simulated realistically the observed SST variability. These studies, together with the complementary studies with atmospheric GCMs forced by observed SSTs [e.g., *Lau*, 1985; *Latif et al.*, 1990], further support that the ENSO phenomenon is predictable.

Finally, the predictability of ENSO was shown in prediction studies. These studies encompass a variety of approaches ranging from purely empirical studies to coupled ocean-atmosphere models. Purely empirical schemes using only atmospheric data as predictors have been developed by *Barnett* [1984], *Barnett et al.* [1988], *Graham et al.* [1987*b*], and *Xu and von Storch* [1990]. While the first three schemes predict future changes in SST, the latter deals with the prediction of the Southern Oscillation Index (SOI) [*Wright*, 1977]. Interestingly, no tropical information is used in the study of *Xu and von Storch* [1990]. An empirical study using heat content variations in the western equatorial Pacific to predict the onset of the 1982/1983 El Niño has been performed by *White et al.* [1987].

Up to now there exist only two physical models which have been used in the predictive mode. The first scheme was developed by *Inoue and O'Brien* [1984]. In this study a linear transport model of the tropical Pacific Ocean is forced by observed winds up to a certain time. Thereafter the winds

Paper number 90JC02468.
0148-0227/91/90JC-02468$05.00

are held constant and the evolution of sea level anomalies at the eastern boundary is investigated. If the sea level anomaly exceeds a certain threshold value, a warm event is declared for the following year. The prediction scheme of *Inoue and O'Brien* [1984] consists therefore only of a yes/no decision for an El Niño event to occur.

In the pioneering studies of *Cane et al.* [1986] and *Cane and Zebiak* [1987] the coupled ocean-atmosphere model of *Zebiak and Cane* [1987] was applied successfully for El Niño predictions. In a later study, *Goswami and Shukla* [1991] determined the full hindcast skill of this coupled model.

In this paper we are concerned with the question as to what degree interannual variability in the tropical Pacific can be understood as a cycle within the coupled ocean-atmosphere system and to what degree the interannual variability is predictable. To answer these questions, we have investigated data from different sources, and we have conducted a large ensemble of prediction experiments with a simplified coupled ocean-atmosphere model.

The paper is basically divided into two parts. In the first part, we investigate the predictability of ENSO by means of data analysis. Our main focus is to answer the question, can ENSO consistently be described as a cycle within the tropical Pacific? The data consist of several years of observed sea levels at Pacific Island stations [*Wyrtki et al.*, 1988], which have recently become available. Sea level fields in the temporal and spatial resolution used here have not been analyzed before, although a similar investigation of sea levels restricted to the western North Pacific has been presented by *Graham and White* [1988]. In addition we analyzed subsurface temperature data simulated with an OGCM when driven with observed wind stresses. These data are of special interest because they are used as initial conditions in the prediction experiments described below. Finally, we analyzed the observed wind stresses themselves. With these data sets we have developed a scenario of how interannual variability evolves in the coupled ocean-atmosphere system.

For our investigation of the interannual variability, we used the new analysis technique of principal oscillation patterns (POPs), which is designed to extract the characteristic space-time variations within a complex multidimensional system [*Hasselmann*, 1988; *von Storch et al.*, 1988; *Xu and von Storch*, 1991]. Although the spatial coverage in the sea level data set is poor in large areas of the equatorial Pacific, we believe that there are enough data to determine the basic spatial characteristics of the interannual sea level variability, which appear to be linked with modes on large spatial scales. Our data analysis strongly supports the hypothesis of *Wyrtki* [1985], according to which, ENSO can be explained as a cycle consisting of an accumulation of warm water in the western Pacific during the cold phases of ENSO and a release of this warm water during the warm phases.

In the second part of the paper, we present a coupled ocean-atmosphere model which has been developed for El Niño predictions and which was systematically used to investigate the predictability of tropical Pacific SST. The philosophy behind the formulation of the coupled ocean-atmosphere model is similar to that of *Cane and Zebiak* [1987]. Following the hypothesis of *Wyrtki* [1985], we assume that the memory of the coupled ocean-atmosphere system is provided entirely by the tropical Pacific Ocean. Therefore the oceanic component is represented by the OGCM described by *Latif* [1987], retaining the full nonlinear ocean dynamics, while the atmospheric component, which has been derived empirically, is assumed to be linear and steady.

Apart from the studies of *Inoue and O'Brien* [1984], *Cane and Zebiak* [1987], and *Goswami and Shukla* [1991], ours is the only study in which a physical model is used to systematically investigate the predictability of the coupled ocean-atmosphere system in the tropical Pacific region with a large ensemble of prediction experiments. Our results suggest that tropical Pacific SST is predictable at lead times of two to three seasons with such a simplified coupled model based on ocean dynamics only. Furthermore, we found SST anomalies least predictable during spring.

This paper is organized as follows: In section 2 we describe the data, the POP method, and the results of the POP analysis. In section 3 we describe the coupled model and its ability to simulate interannual variability. The results of our prediction experiments are presented in section 4. This paper ends with a summary and a discussion of the results in section 5.

2. DATA ANALYSIS

2.1. *Data*

We have investigated the monthly sea levels at Pacific Islands in the region 30°N–30°S for the period 1975–1988 [*Wyrtki et al.*, 1988]. Prior to the analysis the mean annual cycle was subtracted and the data have been projected onto the first nine empirical orthoganal functions (EOFs), which account for 83% of the total variance. The data have not been subjected to any temporal filtering. In addition we analyzed the observed monthly surface wind stress anomalies for the same time period derived from the Florida State University (FSU) data set [*Goldenberg and O'Brien*, 1981; *Legler and O'Brien*, 1984].

Finally, we analyzed the temperature anomalies along the equator in the upper 300 m taken from a simulation with an OGCM forced by the FSU stresses. The ocean model described by *Latif* [1987] is a primitive equation model on an equatorial β plane covering the tropical Pacific Ocean from 30°N to 30°S. It includes real coastlines but no bottom topography, so that the ocean floor is at a constant depth of 4000 m. The longitudinal resolution is constant with 670 km. In the meridional direction the resolution is variable, increasing from 50 km near the equator to about 400 km at the boundaries. Vertically, there are 13 levels, 10 of which are placed within the upper 300 m.

In contrast to *Latif* [1987], we adopt Richardson number dependent vertical mixing coefficients [*Pacanowski and Philander*, 1981]. The vertical eddy viscosity and eddy diffusivity were both assigned values of 20 cm^2/s under neutral conditions and have background values of 0.1 and 0.01 cm^2/s, respectively. The horizontal eddy viscosity is constant with a value of 10^8 cm^2/s. Explicit horizontal heat diffusion is not included.

As is shown in a series of papers, the ocean model simulates reasonably well the observed interannual variability in certain key variables such as SST, zonal currents, and sea level when forced by observed winds [e.g., *Latif*, 1987, 1988; *Latif and Villwock*, 1990; *Barnett et al.*, 1991]. The model nicely reproduces, for instance, the observed east-

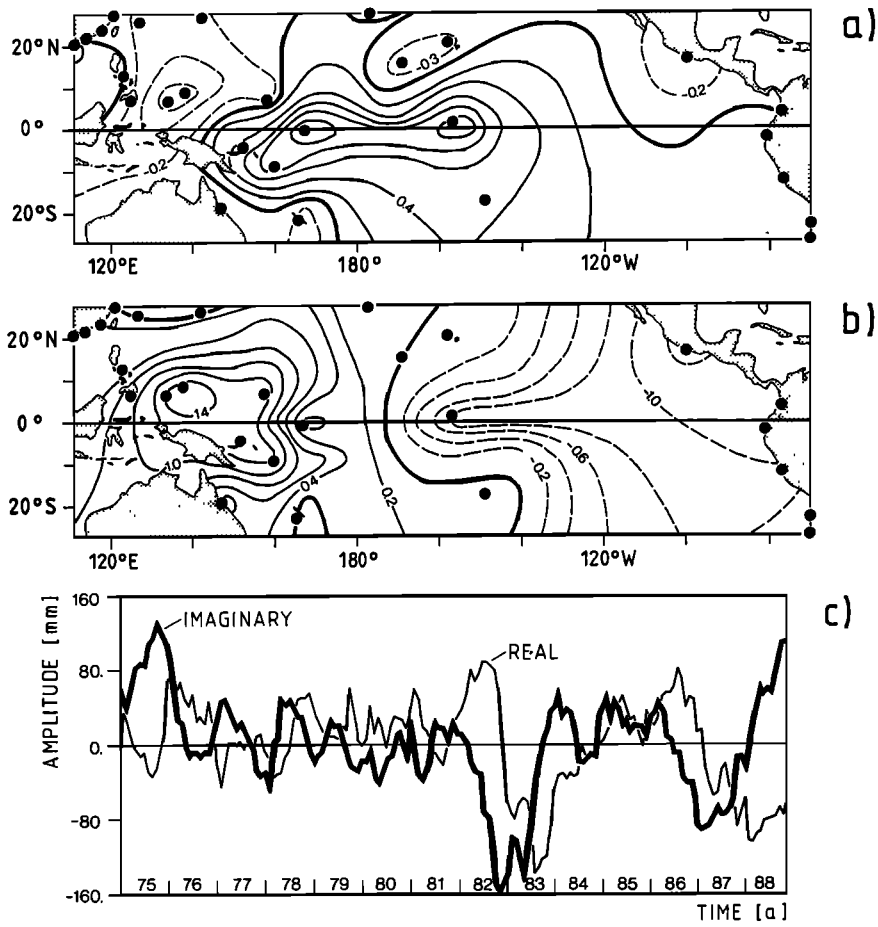

Fig. 1. POP analysis of observed sea level anomalies. The rotation period P of this mode is 40 months with a decay time δ of 16 months. The explained variance amounts to 39%. (*a*) Real part p_1^{SL}. (*b*) Imaginary part p_2^{SL}. Dots show the locations used in the analysis. (*c*) Coefficient time series $z_1^{SL}(t)$ (thin line) and $z_2^{SL}(t)$ (thick line). Units are given in millimeters.

ward propagation of SST during the 1982/183 El Niño. However, the model has the tendency to underestimate the meridional extent of the SST anomalies and to simulate maximum changes in the central rather than in the eastern Pacific. Nevertheless, when the results are averaged over the equatorial Pacific, the agreement with observations is quite good (Figure 8).

2.2. *POP Method*

The analysis is based on the POP method [*Hasselmann*, 1988; *von Storch et al.*, 1988; *Xu and von Storch*, 1990], which is designed to extract the dominant modes of variability within a multidimensional data set. The POPs are the eigenvectors of the system matrix obtained by fitting the data to a multivariate first-order Markov process in which the residual forcing is minimized. In general POPs are complex with real and imaginary parts p_1 and p_2. They can describe traveling modes (when the patterns p_1 and p_2 are approximately in quadrature) or standing waves (when the amplitude of one of the patterns is very small). The complex eigenvalues define a rotation period P and an e-folding time δ for exponential decay. The time evolution of the POPs $(z_1(t), z_2(t))$ is obtained from the projection of the original time series on the adjoint POPs. If the two coefficient time series are in quadrature, as expected theoretically, the evolution of the system in the two-dimensional POP space can be understood as a cyclic sequence of patterns:

$$\cdots \rightarrow p_1 \rightarrow -p_2 \rightarrow -p_1 \rightarrow p_2 \rightarrow \cdots$$

The characteristic anomaly pattern in any other variable y that goes along with the time evolution given by the POP coefficients can be expressed as associated correlation patterns:

$$\langle (y - \hat{z}_1(t)Q_1 - \hat{z}_2(t)Q_2)^2 \rangle \overset{!}{=} \min \hat{z}_i = z_i/\sigma_i \qquad (1)$$

with σ_i being the standard deviation of the coefficient time series $z_i(t)$ and angle brackets denoting expectation. We note that the associated correlation patterns as defined by (1) underestimate the strength of the anomalies by a factor of $2^{1/2}$ during those times when either p_1 or p_2 is observed alone (H. von Storch, personal communication, 1990).

2.3. *Results*

2.3.1. *Observed sea levels and surface stresses.* The POP analysis of observed sea level (SL) anomalies revealed one dominant POP pair (p_1^{SL}, p_2^{SL}) (Figure 1), accounting for 39% of the total variance. The rotation period P of this POP pair is 40 months with a decay time δ of 16 months. All other POPs are exponentially decaying modes with rather small

damping times not being relevant to the ENSO phenomenon. The dominant POP pair is clearly associated with the ENSO phenomenon, which can be inferred from the correlations of the two coefficient time series (Figure 1*c*) with the SOI [*Wright*, 1977]. The zero lag correlation of the coefficient time series $z_2^{SL}(t)$ with the SOI is 0.69, while the 8-months lag correlation of $z_1^{SL}(t)$ with the SOI is 0.52. A cross spectral analysis of the two coefficient time series (not shown) showed the theoretically expected result that they are highly coherent (above the 99% significance level) with a phase shift of about −90° for periods between 20 and 50 months. Therefore low-frequency variability in sea level derived from this single POP pair can be understood as a cyclic sequence of the patterns p_1^{SL} and p_2^{SL}.

As can be inferred from the two coefficient time series (Figure 1*c*), sea level variability during the analyzed period is dominated by the two latest warm episodes, 1982/1983 and 1986/1987, and by the two cold events, 1975 and 1988. Since the POP pair has been rotated in such a way that the coefficient time series $z_2^{SL}(t)$ has maximum correlation with the SOI, pattern p_1^{SL} describes the characteristic anomaly pattern before, pattern $-p_2^{SL}$ describes the characteristic anomaly pattern of sea level during, and pattern $-p_1^{SL}$ the pattern after a warm episode. The pattern p_2^{SL} corresponds to the cold extreme of ENSO.

The pattern p_1^{SL} (Figure 1*a*) can be regarded as a precursor pattern observed during the onset phase of El Niño, preceding the height of the event by a quarter of the rotation period *P*, about 10 months. At this time, strong positive sea level anomalies are found in the western and central Pacific with maxima at the equator. Positive sea level anomalies could already be identified in the western Pacific during the cold phase (pattern p_2^{SL}), but their amplitude is weak, as could be inferred from the corresponding coefficient time series (Figure 1*c*). SST during the onset phase is near normal (not shown). Since sea level is a measure of heat content, this kind of anomaly pattern is consistent with the "pile up" hypothesis of *Wyrtki* [1985].

The associated correlation pattern Q_1^x of the zonal wind stress anomalies (Figure 2*a*) corresponding to pattern p_1^{SL} shows near-normal conditions in the zonal wind stress component along the equator with weak easterly stress anomalies in the eastern part and weak westerly stress anomalies in the western part. The most pronounced signal in the zonal wind stress field off the equator is the relatively strong, spatially coherent westerly anomaly centered at 5°N in the western Pacific extending to 120°W (Figure 2*a*). The meridional structure of this stress anomaly favors Ekman pumping, which could explain the negative sea level anomalies near 10°N (Figure 1*a*). Whether this positive stress anomaly is essential for the initiation of El Niño will be discussed later. The associated correlation pattern for the meridional stress component Q_1^y (not shown) shows at this stage a weak but spatially coherent anomaly pattern with southerly anomalies covering almost the whole equatorial Pacific between 10°N and 10°S.

After a quarter of the rotation period *P*, about 10 months' sea level anomalies are given by pattern $-p_2^{SL}$ (Figure 1*b*), describing the situation during El Niño events with changes in sea level of opposite sign in the western and eastern Pacific. During these warm episodes, sea level anomalies show the well-known reduction of the sea level tilt along the equator [e.g., *Wyrtki*, 1984] with a drop in sea level in the western and a rise in sea level in the eastern equatorial Pacific. The whole pattern is reminiscent of Rossby and Kelvin wave structure. Maximum anomalies in the western Pacific are located on both sides of the equator at about 5°, while anomalies in the east are strongest at the equator and along the coasts of the Americas. Because of the sparcity of the data, we cannot decide to what degree wave reflection is important. However, by following the anomalies from the pattern p_1^{SL} to the pattern $-p_2^{SL}$, one gets some weak indications of Rossby wave reflection at the western boundary and of Kelvin wave reflection at the eastern boundary.

The associated correlation pattern $-Q_2^x$ for the zonal wind stress anomalies during the height of the El Niño event (Figure 2*b*) shows strong westerly anomalies in the western and central Pacific with maximum values at the equator. The strong meridional shear in the zonal wind stress anomaly field roughly coincides with the maxima of the off-equatorial sea level anomalies in the west (Figure 1*b*), as expected from Ekman theory. A similar result is described by *Graham and White* [1988]. Interestingly, the two associated correlation patterns for the zonal wind stress anomalies (Figures 2*a* and 2*b*) are almost identical to the first two low-frequency EOFs of this quantity which were shown to contain the basic ENSO signal [*Latif et al.*, 1990, Figures 7*a* and 8*a*]. This further justifies the discussion of the interannual sea level variability in terms of only a single POP pair. Furthermore,

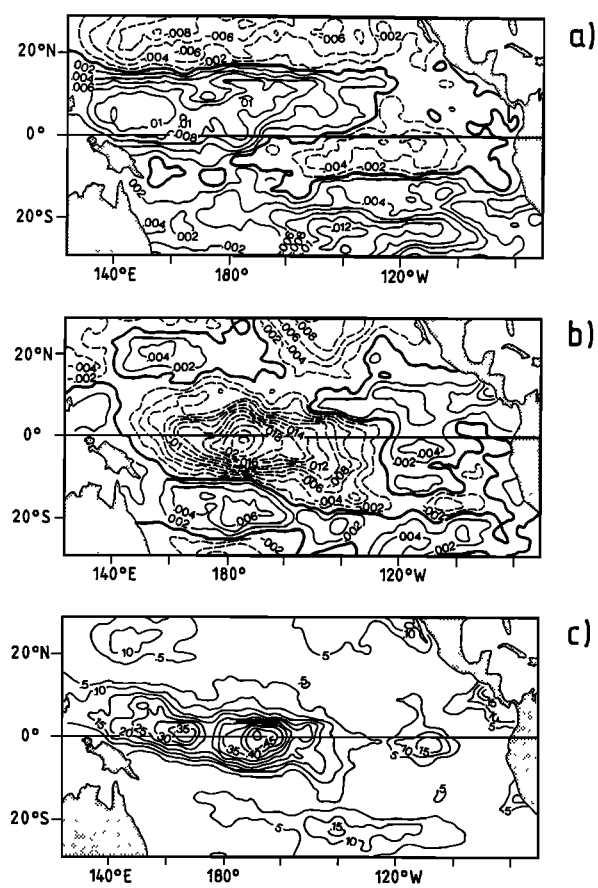

Fig. 2. Associated correlation patterns for the zonal wind stress anomalies for the POP pair shown in Figure 1. (*a*) Pattern Q_1^x, which goes along with the real part p_1^{SL}. (*b*) Pattern Q_2^x, which goes along with the imaginary part p_2^{SL}. (*c*) Variance explained by these two patterns. Units are given in N/m^2.

the explained variances for both the zonal (Figure 2*c*) and meridional wind stress anomalies are in general high, with typical values of 30%–50% in the centers of action.

The characteristic anomaly pattern in the meridional wind stress component $-Q_2^y$ (not shown) during the height of the event shows an equatorward movement of both the intertropical Convergence Zone (ITCZ) and the South Pacific Convergence Zone (SPCZ), a result which has also been obtained by many other authors [e.g., *Rasmusson and Carpenter*, 1982]. The sequence of sea level anomalies is continued with pattern $-p_1^{SL}$, which exhibits negative anomalies at the equator and weaker positive anomalies off the equator.

The described sequence of sea level (or heat content) and surface wind stress anomalies supports the hypothesis that ENSO can be understood as a cycle within the coupled ocean-atmosphere system. During periods of well-developed trade winds, warm water is accumulated in the western Pacific, thereby depressing the thermocline and raising the sea level in this region (Figure 1*a*). This signal could be detected, for instance, prior to the 1986/1987 El Niño in the western Pacific subsurface temperatures, which already showed positive temperature anomalies of the order of 2°C below 140 m in the spring of 1986, about 1 year before the height of the event. During an El Niño event this heat is zonally redistributed, which is clearly reflected in the sea level (Figure 1*b*). This redistribution of heat leads to positive SST anomalies in the eastern Pacific, where the thermocline is shallow. The positive SST anomalies are accompanied by strong westerly wind stress anomalies in the western and central Pacific (Figure 2*b*). After the event the equatorial region is drained of warm water, resulting in lower than normal sea levels, and the trade winds recover, again piling up warm water in the west.

2.3.2. *Upper ocean temperatures derived from an OGCM.* However, due to the sparcity of the investigated sea level data, we do not know to what degree this result is artificial. We have therefore investigated in addition the upper ocean temperatures simulated in our OGCM when driven with observed winds for the period 1961–1985. These temperature data are also of special interest because they serve as initial conditions in the prediction experiments, described below (section 4).

Since the overlapping period with the sea level observations is only 11 years, which is too short to compute reliable estimates of the associated correlation patterns (1) for the dominant POP of observed sea level (Figure 1), we performed a separate POP analysis of the equatorial temperature anomalies in the upper 300 m (Figure 3). We found one dominant POP pair (p_1^T, p_2^T), which accounts for 49% of the total variance. The rotation period P is, with 34 months, somewhat smaller than that of the dominant POP for sea level (P = 40 months), which might be attributed to the different time periods used. The decay time δ is 15 months. This POP mode is also closely related to the ENSO phenomenon: the correlation of the coefficient time series z_2^T (Figure 3*c*) with the SOI is 0.73 and the lag 10 correlation of z_1^T is 0.42. Since the two coefficient time series are highly coherent and in quadrature at periods of 10–50 months (not shown), as expected theoretically, the interpretation of the temperature variability in terms of a cyclic sequence of the two POP patterns (Figures 3*a* and 3*b*) is also justified for this POP mode. All other POPs are statistically insignificant and

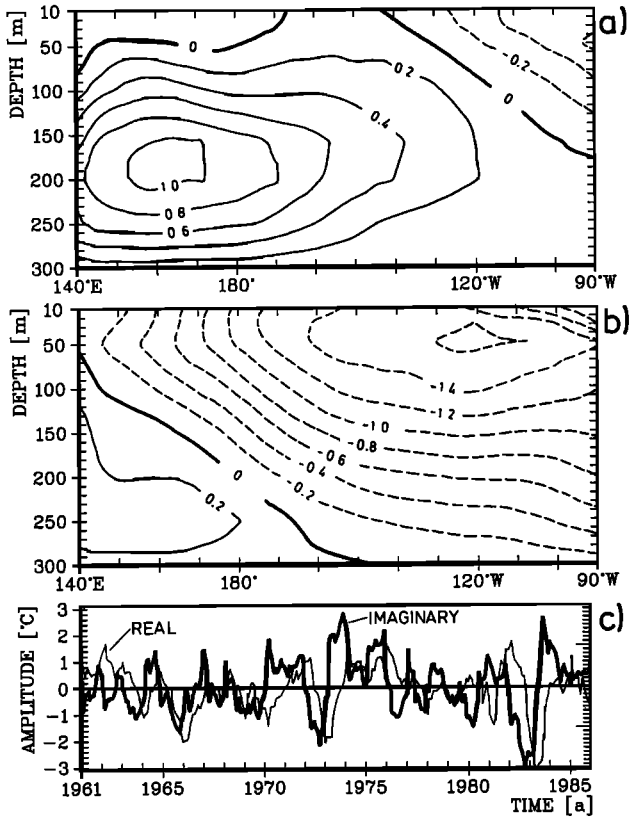

Fig. 3. POP analysis of temperature anomalies in the vertical plane along the equator as simulated in the uncoupled control run with the OGCM forced by observed winds. The rotation period P of this mode is 34 months with a decay time δ of 15 months. The explained variance amounts to 49%. (*a*) Real part p_1^T. (*b*) Imaginary part p_2^T. (*c*) Coefficient time series $z_1^T(t)$ (thin line) and $z_2^T(t)$ (thick line). Units are given in degrees Celsius.

are associated with time scales considerably different from the ENSO time scale.

The pattern p_1^T (Figure 3*a*) again describes the characteristic anomaly pattern during the transition phases, and the patterns p_2^T (Figure 3*b*) that during the extreme phases of ENSO. Several months prior to El Niño events, conditions are given by pattern p_1^T, showing positive temperature anomalies in the western Pacific at subsurface levels between 150 and 250 m, which is consistent with the analysis of observed sea level anomalies (Figure 1*a*). Typical temperature anomalies in the center of action are of the order of 2°C. SST anomalies along the equator are in general weak, being most negative at this stage.

As soon as the subsurface signal has moved far enough to the east to affect the SST because of the shallower thermocline in the eastern Pacific, the coupling with the atmosphere becomes the dominant process. The positive feedback between ocean SST and atmospheric wind stress leads to the well-known warming along the equator with maximum anomalies in the eastern Pacific, as given by pattern $-p_2^T$ (Figure 3*b*). The associated correlation patterns for the zonal surface wind stress anomalies derived from this POP pair (not shown) are almost identical to those shown in Figure 2 and therefore support the assumption that observed and simulated heat content variability are governed by the same mechanism. In summary, the investigation of interannual

variability simulated with our OGCM also supports the pile-up hypothesis of *Wyrtki* [1985] as the dominant ENSO mechanism.

3. COUPLED OCEAN-ATMOSPHERE MODEL

3.1. *Atmospheric Feedback*

Our analysis of the observational data and of the results of the uncoupled run with our OGCM suggests that the memory of the coupled ocean-atmosphere system is governed mostly by the tropical Pacific. Therefore we developed a "minimum" atmospheric model with no dynamics for the use in ENSO prediction experiments, which passively responds to the boundary conditions provided by the ocean. In this model, described by *Latif and Villwock* [1990], the feedback of the atmosphere on the ocean is described by a linear relation between the stress anomaly field τ at each grid point and the local SST anomaly field T:

$$\tau = \tau(T) = \mathbf{a} \cdot T \qquad (2)$$

The set of coefficients $\mathbf{a}$ was determined empirically by a regression analysis using SST anomalies T from the uncoupled ocean model simulation with observed wind stress.

To test the regression method, we reconstructed the stress anomalies τ from the SST anomalies T, simulated in the uncoupled control run with the OGCM forced by observed wind stresses, and compared them with the observed zonal wind stress anomalies derived from the FSU data set. As is shown by *Latif and Villwock* [1990], the correspondence of observed and reconstructed zonal wind stress anomalies along the equator is, in general, good, with best agreement in the western and central Pacific (correlation coefficients r = 0.67 and 0.51, respectively). The lower correlation in the eastern Pacific (r = 0.33) might be attributed to the fact that wind stress is almost "white" in this region [e.g., *Wyrtki*, 1975; *Goldenberg and O'Brien*, 1981] and not well correlated with indices of ENSO.

We have performed in addition an EOF analysis for the reconstructed zonal wind stress anomalies. As has been pointed out, the associated correlation patterns of zonal wind stress anomalies derived from the analysis of observed sea level anomalies (Figure 2) are very similar to the first two low-frequency EOFs of observed zonal wind stress anomalies. Therefore the first two EOFs of the reconstructed fields (Figure 4) can be directly compared here with the associated correlation patterns shown in Figure 2. Together the two EOFs account for about 63% of the total variance in the reconstructed fields.

The EOFs derived from the reconstruction show some correspondence to the patterns derived from the observations. We can identify the big anomaly observed during the extreme phases of ENSO in the western and central Pacific (Figure 2*b*) in the first EOF (Figure 4*a*). However, although the longitudinal position of the maximum is simulated correctly, the meridional extent is seriously underestimated. The second EOF (Figure 4*b*) shows the characteristic north-south asymmetry of anomalies between the western and the eastern equatorial Pacific (Figure 2*a*), but again the meridional extent is much smaller in the reconstructed field.

As shown by *Latif et al.* [1990], the coefficient time series of the first two low-frequency EOFs of the observed zonal wind stress are highly coherent with a constant phase shift of 90°. Therefore the observed variability in the zonal surface stress can be understood as a regular propagation of anomalies from the western into the eastern Pacific. The two EOF coefficient time series derived from the reconstruction with the simple feedback model (Figure 4*c*) show no consistent phase relationship. Furthermore, the time series of the second EOF exhibits only weak interannual variability, being dominated by the 1982/1983 El Niño event. The variability in the reconstructed fields is therefore dominated by a standing component.

3.2. *Extended Range Integration With the Coupled Model*

The OGCM (section 2.1) and the atmospheric feedback model (2) have been coupled by applying an anomaly coupling scheme. The SST anomaly at any given time is determined as the deviation of the actual SST field from the long-term climatology derived from the uncoupled control integration with observed winds. The feedback of the atmosphere is then calculated, applying the simple relationship (2), and the stress anomalies are then added onto the climatological background wind stress to drive the ocean model.

To investigate the variability spectrum of the coupled model, we have forced it by white noise wind stress forcing. That is, each month, we added to the stress anomaly calculated by the regression model (2) a purely zonal spatially coherent stress anomaly, whose time evolution is white. (Without adding noise, the coupled system does not

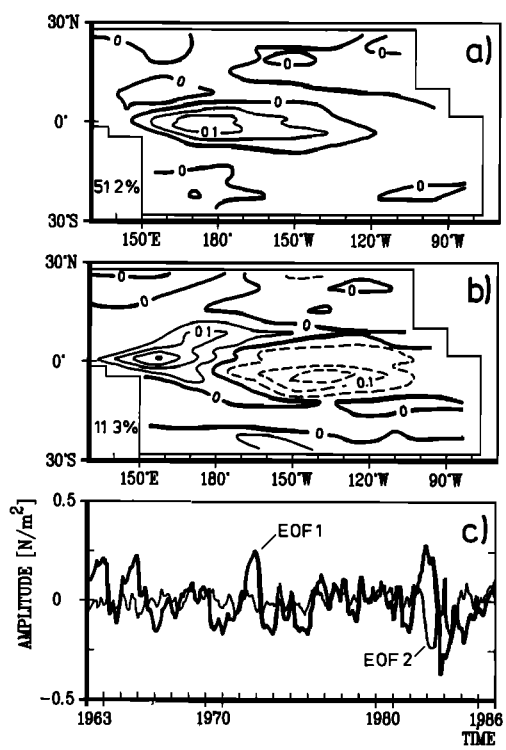

Fig. 4. Reconstruction of zonal wind stress anomalies with the empirical feedback model given by (2) for the period 1963–1986. Shown are the first two leading EOFs of the reconstructed fields. (*a*) First EOF, (*b*) second EOF, (*c*) EOF coefficient time series. The EOFs account for 51.2% and 11.3% of the variance contained in the reconstructed fields. Units are given in N/m^2.

oscillate, while in the case of doubled coupling strength, the coupled model becomes numerically unstable after about 7 years of integration.) As shown by *Latif and Villwock* [1990], the coupled system shows considerable low-frequency variability during a 16-year integration. In particular, the sea level variability as described by the dominant POP pair was found to be similar to the observed variability (Figure 1). For convenience, we have redrawn this POP pair [*Latif and Villwock*, 1990, Figure 7] and present it in Figure 5. This POP accounts for 50% of the total variance in sea level and has a rotation time of $P = 36$ months with a damping time $\delta = 26$ months. It is clearly associated with the low-frequency part of sea level variability, as can be inferred from the coefficient time series (Figure 5*c*). The two POP coefficient time series are highly coherent at low frequencies and show a rather constant phase shift of $-90°$.

Pattern p_1 (Figure 5*a*), being characteristic for the transition phase of the simulated ENSO, exhibits positive anomalies along all of the equator, which is consistent with the observations (Figure 1*a*). Pattern p_2 (Figure 5*b*), describing the situation during the extreme phases of the model ENSO, shows the observed opposite changes in the western and the eastern part with maxima off the equator in the west and one maximum at the equator in the east. Maximum anomalies in the eastern equatorial Pacific are of the order of 15 cm. Westward propagation off the equator and eastward propagation at the equator are clearly visible in this POP pair, which indicates that the propagation of waves as suggested

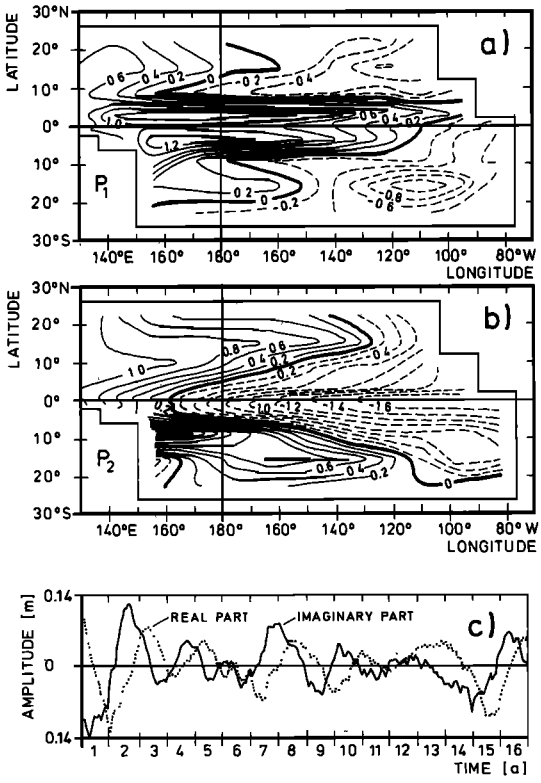

Fig. 5. POP analysis of sea level anomalies simulated in the extended range integration with the coupled ocean-atmosphere when driven with white noise wind stress forcing. The rotation period P of this mode is 36 months with a decay time δ of 26 months. The explained variance amounts to 50%. (*a*) Real part p_1. (*b*) Imaginary part p_2. (*c*) Coefficient time series $z_1(t)$ and $z_2(t)$. Units are given in meters [from *Latif and Villwock*, 1990].

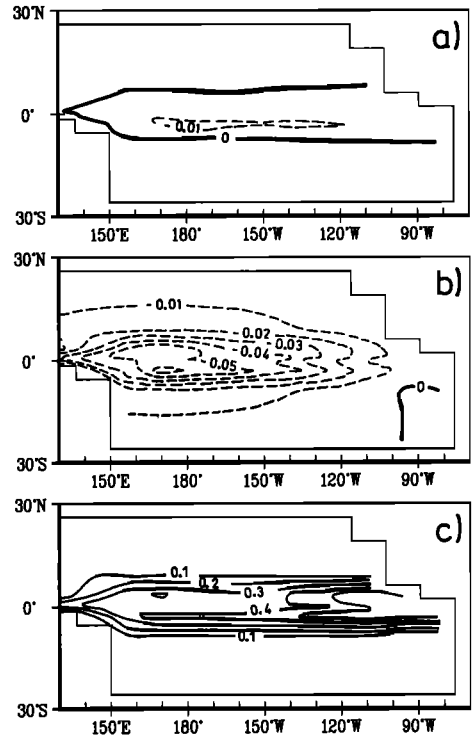

Fig. 6. Associated correlation patterns for the zonal wind stress anomalies simulated in the coupled run for the POP pair shown in Figure 5. (*a*) Pattern Q_1^x, which goes along with the real part p_1. (*b*) Pattern Q_2^x, which goes along with the imaginary part p_2. (*c*) Variance explained by these two patterns. Units are given in N/m^2.

by the "delayed action oscillator" concept plays an important role in the generation of the low-frequency variability.

The associated correlation patterns for the zonal wind stress (Figure 6) and for the subsurface temperature anomalies along the equator (Figure 7) are in many respects very similar to the patterns derived from the observations and from the uncoupled simulations (Figures 2 and 3). Furthermore, the patterns appear to be very stable, as can be inferred from the explained variances, which exceed values of 60% in certain regions (Figures 6*c* and 7*c*). In particular, maximum SST anomalies in the eastern equatorial Pacific, as given by pattern $-Q_2^T$ (Figure 7*b*) were preceded several months earlier by a large-scale subsurface warming centered in the western Pacific, described by pattern Q_1^T (Figure 7*a*). Also, the spatial phase between zonal wind stress and SST anomalies during the extreme phase of the simulated ENSO is realistically simulated (Figures 6*b* and 7*b*).

One important difference to the observations was found in the zonal wind stress which evolves in our coupled simulation as a standing oscillation (Figure 6). As was shown in discussing the variability in the observed zonal wind stresses, positive anomalies in the western Pacific centered north of the equator, observed several months prior to the height of an El Niño (Figure 2*a*), propagate to the east during the event (Figure 2*b*). In our coupled integration, however, anomalous conditions evolve without showing indications of such propagation in the zonal stress field (Figure 6), so that the occurrence of the subsurface warming in the western Pacific (Figure 7*a*) several months prior to the warm phase (Figure 7*a*) must be understood as a delayed response to winds prevailing during the cold phase (Figure

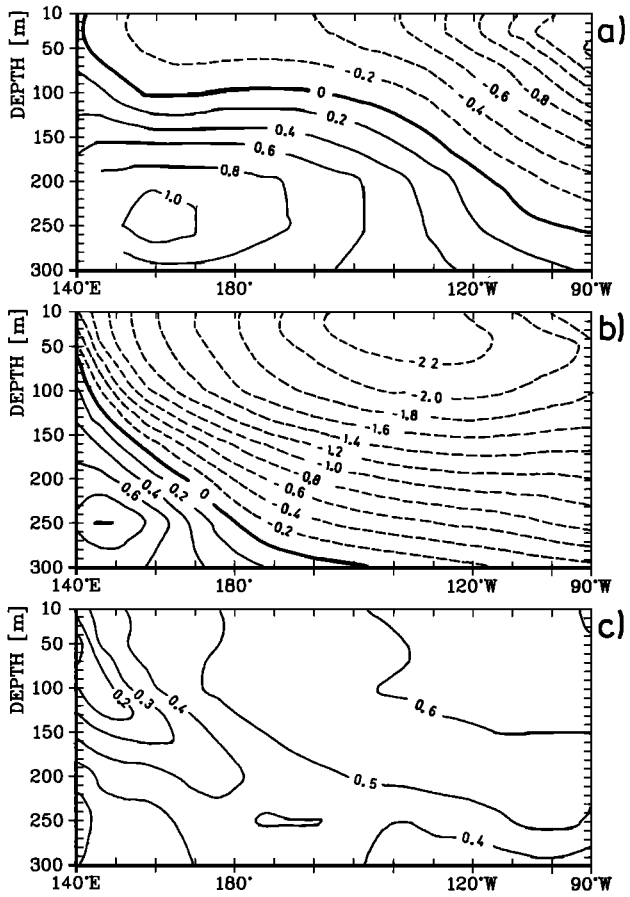

Fig. 7. Associated correlation patterns for the temperature anomalies in the vertical plane along the equator simulated in the coupled run for the POP pair shown in Figure 5. (*a*) Pattern Q_1^T, which goes along with the real part p_1. (*b*) Pattern Q_2^T, which goes along with the imaginary part p_2. (*c*) Variance explained by these two patterns. Units are given in degrees Celsius.

6*b*). This is in contrast to many other studies [e.g., *Barnett*, 1983], in which the eastward propagation of atmospheric anomalies from the Indian Ocean into the central Pacific was shown to be an important contribution to the observed low-frequency variability.

4. Prediction Experiments

Our analysis of the observational data, the uncoupled ocean model results, and the results of the extended range integration with our simplified coupled ocean-atmosphere model have shown that a considerable part of low-frequency variability in the tropical Pacific can be attributed to a cyclic mode similar to the one described by *Wyrtki* [1985]. In particular, anomalies in sea level and SST in the eastern Pacific observed during the extreme phases of ENSO are preceded several months earlier by a characteristic anomaly pattern in upper ocean heat content in the western Pacific. The identification of these characteristic anomaly patterns provides the basis for the experimental prediction of equatorial Pacific SST anomalies, because these anomalies would tend to propagate eastward along the equator even when the winds did not change. Once the heat content anomalies have propagated far enough to the east to affect the SST, the atmospheric feedback becomes important and amplifies the initial signal. Such a scenario seems to be ideal for our simplified coupled ocean-atmosphere model (section 3) because it contains the essential dynamics required for the growth of equatorial SST anomalies within this simple concept. We therefore used it to systematically investigate the predictability of equatorial SST anomalies. For this purpose, we have conducted a large ensemble of prediction experiments to estimate reliable skills for our coupled model.

4.1. *Experimental Setup*

Following the procedure described by *Cane et al.* [1986], the initial conditions for the prediction experiments were taken from an uncoupled control integration with the OGCM, forced by observed wind stresses for the period January 1961 to December 1988 as given by the FSU data set. Predictions have been initialized every third month and have a duration of 2 years. During the integration, the evolution of anomalous conditions is solely determined by the coupled model without adding any further information. We have investigated only the results of the prediction experiments initialized during the period January 1963 to January 1985 to account for the spinup problems and the lack of observed SSTs after 1986. The total number of analyzed predictions is therefore only 89.

We have analyzed instantaneous values of SSTs simulated at the end of each calendar month. Using instantaneous values rather than monthly means can be justified because of the large persistence of the SST anomalies. Comparisons have been performed for an SST index as defined by *Wright* [1985], which is an average over three regions in the equatorial Pacific (6°N–2°N, 170°W–90°W; 2°N–6°S, 180°–90°W; 6°S–10°S, 150°W–110°W) (Figure 8). This SST index was shown to most consistently represent the interannual variability associated with ENSO. The ocean model's performance in the uncoupled control run with observed winds with respect to this SST index is also shown in Figure 8.

The results of the prediction experiments are compared to

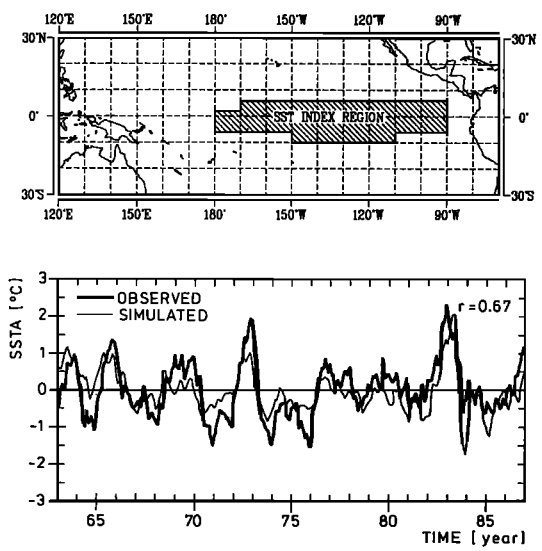

Fig. 8. (Top) Area over which the results of the prediction experiments have been averaged. (Bottom) Comparison of the simulated SST anomalies in the uncoupled control run with observed winds with the observed anomalies averaged over the index region shown in upper panel.

those of the persistence forecast, which assumes the persistence of the initial ocean state, and to those of another set of predictions, hereafter referred to as "persistent wind case," in which the persistence of the initial wind stress field was assumed [*Inoue and O'Brien*, 1984]. As scores, we use the correlation skill and the root mean square (rms) error, which yield measures of the phase and the amplitude error, respectively. We use these two scores instead of the traditional skill [e.g., *Graham et al.*, 1987*b*] because the phase of SST anomalies is much more predictable than their amplitude, as will be shown below.

4.2. *Verification Against Uncoupled Control Run*

In the first step, we verify the results of the prediction experiments against the SST anomalies simulated in the uncoupled control integration with observed winds. By doing so, we simulate a situation in which perfect ocean data are available to initialize the ocean model. The results therefore represent an upper limit for the predictability of tropical Pacific SST anomalies with this particular coupled model.

The correlation skill (Figure 9*a*) demonstrates that the coupled ocean-atmosphere model is in general superior to the persistence forecast. At short lead times, up to 3 months, both the persistence and the coupled model yield reliable forecasts, with the coupled model yielding slightly better correlations. At lead times of two to three seasons, however, the model predictions still yield significant correlations, while the correlations derived from the persistence forecasts are already insignificant. At longer lead times the persistence becomes negative, as expected from the quasi-periodicity of ENSO, and the model gives typical correlations of the order of 0.3, up to lead times of several seasons.

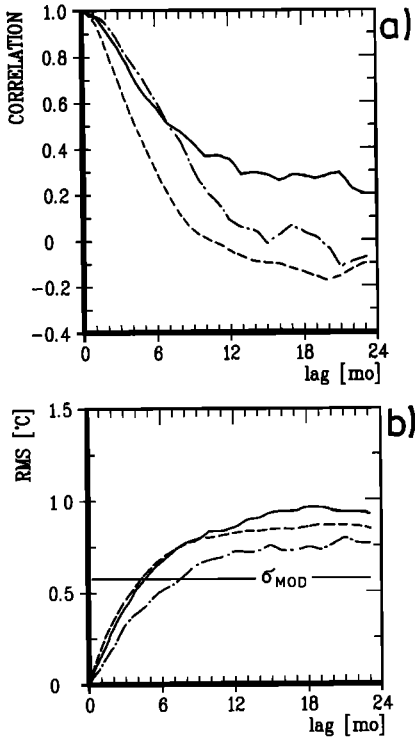

Fig. 9. Prediction of tropical Pacific SST anomalies with the coupled ocean-atmosphere model. (*a*) Correlation and (*b*) rms error, if the scores are calculated verifying the predictions against the SST anomalies simulated in the uncoupled control run with the OGCM driven with observed winds. Dashed lines, persistence; dash-dotted lines, persistent wind case; solid lines, coupled model.

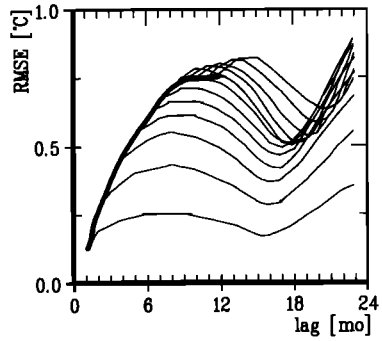

Fig. 10. Growth of small errors (Lorenz curves) for the predictions using initial conditions for successive months for the period 1963–1972. Thin curves show, from bottom to top, the growth of mean 1-month errors, mean 2-month errors, and so on. The heavy curve shows the evolution of the rms error.

The importance of the atmospheric feedback can be inferred from the comparison of the model forecasts with those of the persistent wind case, in which the persistence of the initial surface wind stress field was assumed throughout the forecast period. This set of predictions yields basically the same results as those derived from the coupled model up to lead times of 7 months. Thereafter the coupling becomes important and the correlation skills considerably diverge (Figure 9*a*), with the coupled model giving significantly better results.

The evolutions of the rms error (Figure 9*b*) show rapid initial error growth in all three cases. After 5 months both the coupled model and the persistence error already exceed the standard deviation of the SST anomalies in the index region. The error growth in the persistent wind case is slightly smaller, becoming larger than the standard deviation at lead times of 7 months. After lead times of about 12 months, all three errors reach saturation values, being considerably larger than the standard deviation of the SST anomalies in the uncoupled control run with observed winds.

Following the classical predictability studies of *Lorenz* [1982], we investigated the growth of small initial errors, a method which has been adopted and described in detail by *Goswami and Shukla* [1991] in their investigation of the predictive skill of the coupled model of *Zebiak and Cane* [1987]. In doing so, we carried out another reasonable ensemble of prediction experiments using initial conditions for successive months from the period 1963–1972. Our calculations show that the doubling time of small initial errors is approximately 4 months (Figure 10) with most rapid growth during the first month, which is consistent with the result of *Goswami and Shukla* [1991] who found a doubling time of about 4.5 months. However, in contrast to the findings of Goswami and Shukla, the error does not grow further after it has doubled, but even decreases. This behavior can be attributed to the fact that the coupled model is stable for the parameters chosen, if no external noise is added. For the same reason, large initial errors first tend to decrease and increase later.

In summary, our results suggest that tropical Pacific SST

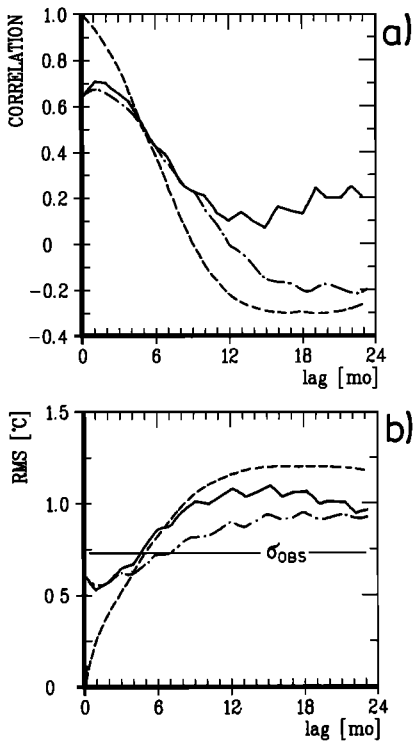

Fig. 11. Prediction of tropical Pacific SST anomalies with the coupled ocean-atmosphere model. (*a*) Correlation and (*b*) rms error, if the scores are calculated verifying the predictions against the observed SST anomalies. Dashed lines, persistence; dash-dotted lines, persistent wind case; solid lines, coupled model.

anomalies are in principle predictable at least up to lead times of about three seasons with our simplified coupled ocean-atmosphere model. Our findings are consistent with those presented by *Goswami and Shukla* [1991], who used the coupled model of *Zebiak and Cane* [1987] in a predictive mode in a large ensemble of experiments.

4.3. *Verification Against Observations*

Our scores drop considerably if we compare the results of the prediction experiments with the observed changes in SST in the index region. As expected, the persistence forecast yields remarkably good results. The autocorrelation does not drop below a value 0.6 before lead times of 5 months (Figure 11*a*). The correlations derived from the coupled model and from the persistent wind case are lower than that of the persistence forecast up to lead times of 4 months. At lead times of 6 months they become superior to the persistence, but the correlations have already dropped to a value of about 0.4. The correlations derived from the coupled model and from the persistent wind case start to diverge at lead of 10 months, with the latter becoming negative after 1 year.

Basically the same kind of behavior is found in the rms error (Figure 11*b*). The persistence error is smaller than the model errors up to lead times of 4 months, while at lead times of 6 months the model errors become smaller. All three errors, however, are already larger than the standard deviation, for lead times larger than 6 months. At lead times of about 12 months the errors begin to saturate.

As can be seen further from the correlation and the rms error, the model predictions suffer from serious errors in the initial conditions. The uncoupled model simulation as expressed by the lag zero statistics exhibits a correlation of the order of 0.65 (the small difference to the correlation given in Figure 8 can be attributed to the fact that we used only every third month), and a rms error which is only slightly smaller than the standard deviation of the observed SST anomalies. These errors in the initial fields can be attributed to systematic errors in the ocean model and to errors in the surface wind stresses used to force the model. It is likely that both errors significantly contribute to the errors in the initial fields.

Although these results are somewhat disappointing, there can be found some promising aspects from the comparisons with the observed SST anomalies (Figure 11). As can be seen from both the correlation and the rms error, the slopes of the model curves are significantly different from those derived from persistence: at lead times up to about 1 year, the correlation drops and the rms error grows at a smaller rate. Therefore it might be possible to increase the skill of our coupled model with respect to observations just by constructing a less flawed initial field. Since we have not used any ocean observations to initialize the ocean model, the assimilation of certain available ocean observations, such as SST and sea level, might be sufficient to significantly increase the skill of our model.

4.4. *Seasonality*

We have further investigated the predictability of tropical Pacific SST anomalies by computing the scores as functions of the season. Since we have initialized predictions every third month, scores can be calculated only for January, April, July, and October. By doing so, the number of entries for each subset reduces to a maximum of 23, so that the results have to be interpreted with some caution. Nevertheless, we believe that we can identify the basic aspects of the seasonal dependence of the predictability with these rather small ensembles.

We present in Table 1 the correlation skills as functions of the month of initialization and as functions of the lead time, if the results are verified against those simulated in the uncoupled control run. Because we are interested only in the gross features and because of the small ensemble of predictions, we show the correlations only for lead times 2 months apart from each other and with an accuracy of 0.1. If a threshold value of 0.6 is adopted, being representative for reliable predictions, it can be inferred from Table 1 that SST anomalies in late spring and early summer are least predict-

TABLE 1. Correlation Coefficients of the SST Anomalies Predicted With the Coupled Model With the SST Anomalies Simulated in the Uncoupled Control Run With Observed Winds

	Lag, months							
Month	1	3	5	7	9	11	13	15
Jan.	1.0	0.7	0.5	0.4	0.3	0.6	0.6	0.3
April	1.0	0.8	0.6	0.5	0.6	0.4	0.1	0.2
July	1.0	0.8	0.8	0.8	0.5	0.3	0.2	0.1
Oct.	1.0	0.9	0.6	0.4	0.3	0.1	0.2	0.5

Correlations are given as a function of the month of initialization and the forecast lag.

TABLE 2. Correlation Coefficients of the SST Anomalies Predicted With the Coupled Model With the Observed SST Anomalies

	Lag, months							
Month	1	3	5	7	9	11	13	15
Jan.	0.7	0.6	0.2	0.1	0.1	0.3	0.3	0.2
April	0.7	0.7	0.6	0.5	0.4	0.3	0.1	−0.1
July	0.9	0.7	0.8	0.6	0.4	0.0	0.0	0.0
Oct.	0.8	0.7	0.5	0.3	0.1	0.0	0.1	0.2

Correlations are given as a function of the month of initialization and the forecast lag.

able. One exception is found for the predictions initialized in April, which show a drop below a correlation of 0.6 at a lead time of 7 months (November). However, we believe that this feature can be attributed to the small sample size. This is supported by the fact that the correlation increases again at a lead time of 9 months.

The most predictable SST anomalies are those during the winter months. Most impressive for the predictions starting in January is the recovery of the correlation skill during the following winter, when the persistence forecast yields insignificant correlations (not shown). Basically the same kind of behavior is found for the rms error (not shown): the error growth is largest in spring and smallest in winter.

The same basic behavior is found for the predictability of observed SST anomalies (Table 2). Although the correlations are in general smaller than those presented in Table 1, the dependence on season is similar. For predictions starting in July, for instance, the skill does not drop below 0.6 until March. These results are consistent with the findings of *Wright* [1895], who investigated the persistence of observed SST anomalies and with the results of *Graham et al.* [1987*b*], who used an empirical prediction scheme based on surface winds as predictors.

5. SUMMARY AND DISCUSSION

We have investigated the short-range climate predictability in the tropical Pacific using data from different sources and a simplified coupled ocean-atmosphere model in a large ensemble of prediction experiments. We addressed two questions. First, to what degree can interannual variability in the tropical Pacific be understood as a cycle within the coupled ocean-atmosphere system? Second, to what degree are low-frequency changes in equatorial SST predictable?

We draw two main conclusions from this study:

1. A significant contribution to interannual variability in the tropical Pacific can be understood as a cycle within the coupled ocean-atmosphere system.
2. SST anomalies are predictable at lead times of two to three seasons with our simplified coupled ocean-atmosphere model with best skills predicting SST anomalies in winter and worst skills predicting SST anomalies in spring.

The statistical investigation of observed sea levels strongly supports the hypothesis of *Wyrtki* [1985], according to which ENSO can be understood as a cycle within the coupled ocean-atmosphere system consisting of a slow accumulation of warm water by the trade winds in the western Pacific during the cold phases of ENSO and a subsequent loss of this heat toward higher latitudes during the warm phases. The oscillation period can be understood within this concept as the time required to refill the reservoir of warm water in the western Pacific. Basically the same mechanism was found by *Cane and Zebiak* [1987], who investigated the low-frequency variability simulated in a simplified coupled ocean-atmosphere model.

As shown in Figure 1, one POP mode alone, which describes such a cycle in observed sea level, accounts for about 40% of the unfiltered variance. The analyzed sea level data set, covering only the period 1975–1988, is certainly not long enough and has too little spatial coverage to exclude serious artificial skills. However, our companion analysis of the observed surface wind stresses (Figure 2) and of the subsurface temperatures simulated in our OGCM when forced by observed winds (Figure 3) further supports the hypothesis of *Wyrtki* [1985]. In particular, the subsurface temperatures simulated in the vertical plane along the equator show a characteristic anomaly pattern consisting of a large-scale subsurface warming several months before the height of El Niño events. As can be inferred from recent measurements of subsurface temperatures in the western equatorial Pacific, a subsurface warming was indeed observed several months prior to the 1987 El Niño event.

Although all El Niños were preceded by the subsurface warming in the western Pacific described above (Figures 1*c* and 3*c*), there are also a few times when the precursor pattern was well developed but not followed by an El Niño, namely, in 1962 and 1974. The subsurface warming in the west can therefore not be regarded as a sufficient condition for an El Niño to occur. Furthermore, the strength of the subsurface warming does not seem to be correlated with the strength of the following event. As can be inferred from the investigation of observed sea levels, both the 1982/1983 and the 1986/1987 El Niños were preceded by heat content anomalies of about the same strengths (Figure 1*c*). The strengths of the following events, however, were very different, with the 1982/1983 event being the most pronounced warm event during this century and almost twice as strong as the 1986/1987 event.

The ENSO mechanism described above does not require any low-frequency forcing from the atmosphere [*Wyrtki*, 1985]. As discussed by *Cane and Zebiak* [1987], the presence of high-frequency but spatially coherent atmospheric disturbances, such as the "30–60 day" oscillation [*Madden and Julian*, 1971], would be sufficient to initiate El Niño events. The results of the extended range integration with the coupled model (Figures 5, 6, and 7), which by definition does not contain any atmospheric dynamics, show that variability patterns similar to those observed can be simulated based on ocean dynamics only. This result is inconsistent with observations of sea level pressure and low-level winds. Several authors [e.g., *Barnett*, 1983; *Graham et al.*, 1987*a*, *b*; *von Storch et al.*, 1989] have shown that a distinct propagation of atmospheric anomalies exists from the Indian Ocean eastward into the Pacific area. Further, *Barnett et al.* [1991] found a significant nonlinear interaction of such a progressive mode with a standing Pacific mode in sea level pressure. Here, we cannot give a satisfactory answer as to what degree the progressive atmospheric mode found in other studies is important in forcing low-frequency variability in the tropical Pacific. The neglect of any processes outside the tropical Pacific therefore might significantly limit the predictability of tropical Pacific SST.

Nevertheless, our data analysis confirms that the state of the tropical ocean-atmosphere system is, in principle, predictable a few seasons ahead. This is supported by analyzing the results of a large ensemble of prediction experiments with our simplified coupled ocean-atmosphere model, neglecting any atmospheric dynamics. We first compared the SST anomalies simulated in the prediction experiments with those simulated in the uncoupled control integration with the OGCM with observed winds. By doing so, we simulate a situation in which perfect initial conditions are available. Tropical Pacific SST anomalies can be predicted in such a situation at lead times of several months (Figure 9). The skill could probably even be increased by using, instead of our "minimum atmospheric model," which includes only an empirically derived linear and local feedback (2), a more sophisticated atmosphere model.

We found a pronounced dependence of the scores on the season, with SSTs in spring being least and SSTs in winter being most predictable (Table 1). It is interesting that these results were obtained without including any seasonal dependence in the atmospheric feedback.

Although our prediction experiments have been performed in the hindcast mode, in the sense that the feedback coefficients were derived from the same time period for which the predictions were conducted, we believe that our skills are close to the "true" skill of our coupled system. Deriving the feedback coefficients from different time periods yielded essentially identical results within the latitude band 10°N–10°S. Since the feedback coefficients are, besides the annual cycles of SST and surface wind stress, the only "dependent" quantities in our prediction studies, there should be almost no artificial skill in our results.

The comparison of the results of the prediction experiments with observed SST changes showed that the coupled model in its present version is not well suited for use in a real forecast situation, if the results are averaged over all seasons. At lead times up to 5 months the coupled model yields skillful predictions (Figure 11), but we found the persistence forecast giving even better scores at these lags. Although the model predictions exhibit better scores at longer lead times, the scores are below the limits for reliable predictions. In certain seasons, however, reliable predictions are possible at lead times up to 7 months, with best skills for predictions initiated in July (Table 2).

As was shown, the predictions suffer partly from serious errors in the initial conditions, which are of the order of the standard deviation of the observed SST anomalies themselves. These errors can be attributed mostly to systematic errors in the ocean model and to errors in the wind stresses used to force the ocean model. On the other hand, it was shown that the drop of the correlation skill and the growth in rms error were considerably smaller than for the persistence forecast. Thus the construction of better initial fields, if consistent with the dynamics of the ocean model, could significantly increase our skill.

We have therefore investigated the systematic errors in the uncoupled control integration with the OGCM forced by observed winds. The errors in the simulated SST anomalies in the equatorial zone 5°N–5°S were found to be strongly correlated with the simulated SST anomalies themselves. Typical correlations are of the order of 0.7 in the western and central Pacific with maximum values up to 0.9 at certain locations. Since the fields simulated in the uncoupled control integration are used as initial conditions for the prediction experiments, these results indicate that the simulation, and therefore the initial fields, can be significantly improved at least by means of an empirical correction scheme to yield better predictions.

Another possibility of improving the quality of the initial conditions is the assimilation of observations into the ocean model. As was shown by *Philander et al.* [1987], the most important quantity required to represent the oceanic state in the equatorial Pacific is subsurface temperature within the thermocline. *Philander et al.* [1987] showed that only a few meridional sections across the equatorial Pacific are needed, because of the large spatial scales involved. Since subsurface information in the required spatial and temporal resolution is not available in near real-time at present, we have to seek other available ocean observations. At present there are only two quantities available in near real-time, SST [*Reynolds*, 1988] and sea level at Pacific Islands [*Wyrtki et al.*, 1988]. SST could be simply used instead of the climatological air temperature in our heat flux parameterization to force the ocean model toward the observed state. However, by doing so, it has to be assured that this procedure is consistent with the dynamics of the ocean model. Otherwise the error growth within our coupled system would become larger, and the advantage of a better initial field could be cancelled out. Sea level data cannot be used in such a direct way, since they have to be consistent with the density structure of the model. With respect to sea level, we therefore have to develop a sophisticated assimilation scheme.

Acknowledgments. We wish to thank K. Hasselmann for suggesting the use of an empirical atmospheric feedback in coupled ocean-atmosphere models. We are indebted to J.-S. Xu for providing the POP analyses of the observed sea levels. Many thanks to H. von Storch and E. Maier-Reimer for many fruitful discussions. We are indebted to J. J. O'Brien for providing the wind stress data and to K. Wyrtki for providing the sea level data. We would like to thank one anonymous reviewer for suggesting the investigation of the growth of small errors. We would like to thank P. B. Wright for providing the SST index and for editing the English and A. Schwarz for programming assistance. Thanks also to M. Grunert and to D. Lewandowski for preparing the diagrams. This study was partly financed by the European Community Climate Program under grant EV4C-0035-D(B).

REFERENCES

Barnett, T. P., Interaction of the monsoon and Pacific trade wind system on interannual time scales, I, The equatorial zone, *Mon. Weather Rev.*, *111*, 756–773, 1983.

Barnett, T. P., Prediction of the El Niño 1982–83, *Mon. Weather Rev.*, *112*, 1403–1407, 1984.

Barnett, T., N. Graham, M. Cane, S. Zebiak, S. Dolan, J. O'Brien, and D. Legler, On the prediction of the El Niño 1986–1987, *Science*, *241*, 192–196, 1988.

Barnett, T. P., M. Latif, E. Kirk, and E. Roeckner, On ENSO physics, *J. Clim.*, in press, 1991.

Battisti, D. S., Dynamics and thermodynamics of a warming event in a coupled atmosphere-ocean model, *J. Atmos. Sci.*, *45*, 2889–2919, 1988.

Bjerknes, J., Atmospheric teleconnections from the equatorial Pacific, *Mon. Weather Rev.*, *97*, 163–172, 1969.

Busalacchi, A. J., and J. J. O'Brien, Interannual variability of the equatorial Pacific in the 1960s, *J. Geophys. Res.*, *86*(C11), 10,901–10,907, 1981.

Busalacchi, A. J., K. Takeuchi, and J. J. O'Brien, Interannual variability of the equatorial Pacific, in *Hydrodynamics of the*

Equatorial Ocean, Oceanogr. Ser. 36, edited by J. C. J. Nihoul, Elsevier, New York, 1983.

Cane, M. A., El Niño, *Annu. Rev. Earth Planet. Sci.*, *14*, 43–70, 1986.

Cane, M. A., and S. E. Zebiak, Prediction of El Niño events using a physical model, in *Atmospheric and Oceanic Variability*, edited by H. Cattle, Royal Meteorological Society, James Glaisher House, Bracknell, England, 1987.

Cane, M. A., S. E. Zebiak, and S. C. Dolan, Experimental forecasts of El Niño, *Nature*, *321*, 827–832, 1986.

Goldenberg, S. O., and J. J. O'Brien, Time and space variability of tropical Pacific wind stress, *Mon. Weather Rev.*, *109*, 1190–1207, 1981.

Goswami, B. N., and J. Shukla, Predictability of a coupled ocean-atmosphere model, *J. Clim.*, in press, 1991.

Graham, N. E., and W. B. White, The El Niño cycle: A natural oscillator of the Pacific Ocean-atmosphere system, *Science*, *240*, 1293–1302, 1988.

Graham, N. E., J. Michaelsen, and T. P. Barnett, An investigation of the El Niño–Southern Oscillation cycle with statistical models, 1, Predictor field characteristics, *J. Geophys. Res.*, *92*(C13), 14,251–14,270, 1987*a*.

Graham, N. E., J. Michaelsen, and T. P. Barnett, An investigation of the El Niño–Southern Oscillation cycle with statistical models, 2, Model results, *J. Geophys. Res.*, *92*(C13), 14,271–14,289, 1987*b*.

Hasselmann, K., PIPs and POPs: The reduction of complex dynamical systems using principal interaction and oscillation patterns, *J. Geophys. Res.*, *93*(D9), 11,015–11,021, 1988.

Inoue, M., and J. J. O'Brien, A forecasting model for the onset of El Niño, *Mon. Weather Rev.*, *112*, 2326–2337, 1984.

Latif, M., Tropical ocean circulation experiments, *J. Phys. Oceanogr.*, *17*, 246–263, 1987.

Latif, M., ENSO modelling at MPI, *Rep. 22*, Max-Planck-Institut für Meteorologie, Hamburg, Federal Republic of Germany, 1988.

Latif, M., and A. Villwock, Interannual variability as simulated in coupled ocean-atmosphere models, *J. Mar. Syst.*, *1*, 51–60, 1990.

Latif, M., J. Biercamp, H. von Storch, M. J. McPhaden, and E. Kirk, Simulation of ENSO related surface wind anomalies with an atmospheric GCM forced by observed SST, *J. Clim.*, *3*, 509–521, 1990.

Lau, N. C., Modeling of the seasonal dependence of the atmospheric response to observed El Niños in 1962–76, *Mon. Weather Rev.*, *113*, 1970–1996, 1985.

Legler, D. M., and J. J. O'Brien, Atlas of tropical Pacific wind stress climatology 1971–1980, 182 pp., Fla. State Univ., Dep. of Meteorol., Tallahassee, 1984.

Lorenz, E. N., Atmospheric predictability experiments with a large numerical model, *Tellus*, *34*, 505–513, 1982.

Madden, R. A., and P. R. Julian, Detection of a 40–50 day oscillation in the zonal wind in the tropical Pacific, *J. Atmos. Sci.*, *28*, 702–708, 1971.

McCreary, J. P., A model of tropical ocean-atmosphere interaction, *Mon. Weather Rev.*, *111*, 370–387, 1983.

Pacanowski, R. C., and S. G. H. Philander, Parameterization of vertical mixing in numerical models of tropical oceans, *J. Phys. Oceanogr.*, *11*, 1443–1451, 1981.

Philander, S. G. H., and A. D. Seigel, Simulation of El Niño of 1982–1983, in *Coupled Ocean-Atmosphere Models, Oceanogr. Ser. 40*, edited by J. C. J. Nihoul, Elsevier, New York, 1985.

Philander, S. G. H., W. J. Hurlin, and R. C. Pacanowski, Initial conditions for a general circulation model of tropical oceans, *J. Phys. Oceanogr.*, *17*, 147–157, 1987.

Rasmusson, E. N., and T. H. Carpenter, Variations in tropical sea surface temperature and surface wind fields associated with the Southern Oscillation/El Niño, *Mon. Weather Rev.*, *110*, 354–384, 1982.

Reynolds, R. W., A real-time global sea surface temperature analysis, *J. Clim.*, *1*, 75–86, 1988.

Schopf, P. S., and M. J. Suarez, Vacillations in a coupled ocean-atmosphere model, *J. Atmos. Sci.*, *45*, 549–566, 1988.

Seager, R., Modeling tropical Pacific sea surface temperature: 1970–87, *J. Phys. Oceanogr.*, *19*, 419–434, 1989.

von Storch, H., T. Bruns, I. Fischer-Bruns, and K. Hasselmann, Principal Oscillation analysis of the 30- to 60-day oscillation in a GCM, *J. Geophys. Res.*, *93*(D9), 11,022–11,036, 1988.

von Storch, H., U. Weese, and J. S. Xu, Simultaneous analysis of space-time variability: Principal oscillation patterns and principal interaction patterns with applications to the Southern Oscillation, *Rep. 34*, Max-Planck-Institut für Meteorologie, Hamburg, Federal Republic of Germany, 1989.

White, W. B., S. E. Pazan, and M. Inoue, Hindcast/forecast of ENSO events based upon the redistribution of observed and model heat content in the western tropical Pacific, 1964–86, *J. Phys. Oceanogr.*, *17*, 264–280, 1987.

Wright, P. B., The Southern Oscillation—Patterns and mechanisms of the teleconnections and the persistence, *Rep. HIG 77-13*, Hawaii Inst. of Geophys. Univ. of Hawaii, Honolulu, 1977.

Wright, P. B., The Southern Oscillation: An ocean-atmosphere feedback system?, *Bull. Am. Meteorol. Soc.*, *66*, 398–412, 1985.

Wyrtki, K., El Niño—The dynamic response of the equatorial Pacific Ocean to atmospheric forcing, *J. Phys. Oceanogr.*, *5*, 572–584, 1975.

Wyrtki, K., The slope of sea level along the equator during the 1982/1983 El Niño, *J. Geophys. Res.*, *89*(C4), 10,419–10,424, 1984.

Wyrtki, K., Water displacements in the Pacific and the genesis of El Niño cycles, *J. Geophys. Res.*, *90*(C4), 7129–7132, 1985.

Wyrtki, K., K. Constantine, B. J. Kilonsky, G. Mitchum, B. Miyamoto, T. Murphy, S. Nakahara, and P. Caldwell, The Pacific Island sea level network, *JIMAR Contrib. 88-0137, Data Rep. 002*, Univ. of Hawaii, Honolulu, 1988.

Xu, J. S., and H. von Storch, Principal oscillation patterns—Prediction of the state of ENSO, *J. Clim.*, in press, 1990.

Zebiak, S. E., and M. A. Cane, A model El Niño–Southern Oscillation, *Mon. Weather Rev.*, *115*, 2262–2278, 1987.

M. Flügel and M. Latif, Max-Planck-Institut für Meteorologie, Bundesstrasse 55, D-2000 Hamburg 13, Federal Republic of Germany.

(Received June 15, 1990;
revised October 8, 1990;
accepted October 24, 1990.)